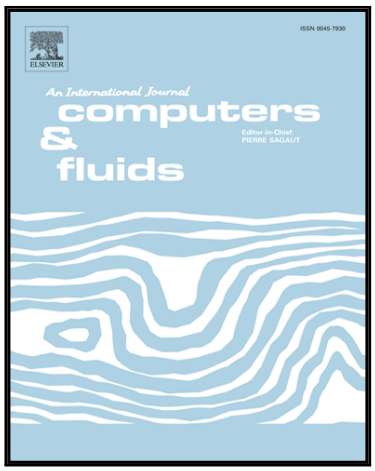

Seventh order hermite weno scheme for hyperbolic conservation laws

Yousef Hashem Zahran , Amr H. Abdalla

PII: S0045-7930(16)30064-0
DOI: 10.1016/j.compfluid.2016.03.010
Reference: CAF 3116

To appear in: *Computers and Fluids*

Received date: 29 July 2015
Revised date: 12 January 2016
Accepted date: 10 March 2016

Please cite this article as: Yousef Hashem Zahran , Amr H. Abdalla , Seventh order hermite weno scheme for hyperbolic conservation laws, *Computers and Fluids* (2016), doi: 10.1016/j.compfluid.2016.03.010

.

Highlights

- A new seventh Hermite WENO scheme for solving hyperbolic conservation laws.
- The major advantage of HWENO scheme is its compactness in the reconstruction.
- It uses the central upwind flux presented by Kurganov which is simple, universal and efficient.
- For time integration, we (ℓSSPRK 7) for linear problems and SSPRK54 for nonlinear. 7SSPRK□
- The advantages: improvement the accuracy of smooth parts, decreases the dissipation near discontinuities and can be used for problems with non-convex fluxes.

SEVENTH ORDER HERMITE WENO SCHEME FOR HYPERBOLIC CONSERVATION LAWS

Yousef Hashem Zahran, Amr H. Abdalla

Physics and Mathematics Department

Port Said University, Faculty of Engineering, Port Said, Egypt,

dryhhz@yahoo.com

Abstract

In this paper, we construct a new seventh order Hermite weighted essentially non-oscillatory (HWENO7) scheme, for solving one and two dimensional hyperbolic conservation laws, by extending the fifth order HWENO introduced in [J. Qiu, Shu, C.-W.. J. Comput. Phys. **193**, 115–135 (2003)]. The idea of the reconstruction in the HWENO schemes comes from the original WENO schemes, however both function and its derivative values are evolved in time and used in the reconstruction, while only the function values are evolved and used in the original WENO schemes. The major advantage of HWENO schemes is its compactness in the reconstruction. For example, seven points are needed in the stencil for a seventh order WENO reconstruction, while only five points are needed for HWENO7 reconstruction. We use the central-upwind flux [Kurganov, A., Noelle, S., and Petrova, G., SIAM J. Sci. Comp. 23 (2001), pp.707–740] which is simple, universal and efficient. The numerical solution is advanced in time by the seventh order linear strong-stability-preserving Runge-Kutta (ℓSSPRK) scheme for linear problems and the fourth order SSPRK(5,4) for nonlinear problems.The resulting scheme improves the convergence and accuracy of smooth parts of solution as well as decrease the dissipation near discontinuities. This is especially for long time evolution problems. Numerical experiments of the new scheme for one and two dimensional problems are reported. The results demonstrate that the proposed scheme is superior to the original HWENO and classical WENO schemes.

Key words: Conservation laws, Hermite WENO, central-upwind flux, ℓSSPRK Runge-Kutta, Euler equations, Burgers equation.

1. Introduction

In this paper we design seventh order HWENO scheme for solving one and two dimensional hyperbolic conservation laws

$$u_t + \nabla . f(u) = 0, \quad u(x,0) = u_0(x), \qquad x \in (-\infty, \infty), t \in (0, \infty) \tag{1.1}$$

This equation can be scalar or system and it is often nonlinear.

Hyperbolic conservation laws (1.1) play an important role arise in applications, such as gas dynamics, weather prediction, rarefied gas dynamics and many others. It is well known that the solutions of hyperbolic conservation laws may develop discontinuities even when the initial condition is smooth and therefore the numerical methods should compute such discontinuities with correct position and without oscillations and yet achieve high order of accuracy in smooth regions. Amongst successful development in this direction we have total variation diminishing (TVD) methods [5] and weighted essentially non-oscillatory (WENO) methods. WENO schemes are based upon the successful essentially non-oscillatory (ENO) schemes started with the henceforth classic paper of Harten et al [6] and have been improved by Jiang and Shu [8] and many others e.g.,[2], [7] and [17]. Finite difference WENO schemes of higher orders (seventh to eleventh order) are constructed in [1]. WENO schemes have the following advantages: uniform high order accuracy in smooth regions including at smooth extreme, unlike second order TVD schemes which degenerate to first order accuracy at smooth extreme; sharp and non-oscillatory (to the eyes) shock transition; robust for many physical systems with strong shocks and especially suitable for simulating solutions containing both discontinuities and complicated smooth solution structure, such as shock interaction with vortices.

Nevertheless, in spite of the vast applications of WENO schemes, they still have deficiencies: numerical tests indicate that the classical WENO schemes are usually not optimal for computing turbulent flows or aero-acoustic fields because they can lead to a significant damping of the turbulent or acoustic fluctuations; due to the width of their numerical stencil, the extension to non-Cartesian meshes is somewhat cumbersome; moreover, a wide stencil is not optimum neither in terms of an accurate treatment of weak fluctuations, nor concerning the imposition of boundary conditions.

A way to improve the dissipation properties of the WENO schemes consists in reducing its stencil width. Indeed, the compactness of a numerical stencil owes many advantages: firstly, boundary conditions and complex geometries are easier to deal with; secondly, for the same formal accuracy, compact stencils are known to exhibit significantly more resolution of the smaller scales by improving the dispersive and dissipative properties of the numerical schemes.

In [14], following the idea of WENO, Qui and Shu presented of Hermite WENO (HWENO) schemes. The idea of the reconstruction in the HWENO schemes comes from the original WENO schemes, however both the function and its derivative values are evolved in time and used in the reconstruction, while only the function value are evolved and used in the original WENO schemes. Comparing with the original WENO schemes of Jiang and Shu [8], one major advantage of HWENO schemes is its compactness in the reconstruction. For example, five points are needed in the stencil for the fifth order WENO schemes, while only three points are needed for a fifth order HWENO schemes. In [3], Capdeville constructed a sixth order HWENO scheme for solving one dimensional hyperbolic conservation laws. This scheme lies upon a central and local Hermite WENO interpolation. In [15], HWENO schemes were extended to solve two dimensional conservation laws. Recently, in [13], Tao et al proposed a class of fifth order schemes for solving one dimensional hyperbolic conservation laws while fourth order for two dimensions. The methods involved HWENO reconstruction in space and Lax-Wendroff type discretization in time. In [11], a class of HWENO schemes is presented which based on a finite difference formulation. In [12], Liu and Qui presented an alternative approach to construct the numerical fluxes, in which they used the solution and its derivatives directly to interpolate point values at the interfaces of computational cells and then put the point values in the building block to generate numerical flux.

The purpose of this paper is three fold. Firstly, we construct a new seventh order HWENO interpolation procedure. The interpolation results from extending the fifth order HWENO scheme [14]. Secondly, we propose to use a more general Central-Upwind flux introduced in [9,10] which is simple, universal and efficient scheme. Thirdly, for the time integration we use the seventh order linear strong-stability-preserving Runge-Kutta (ℓSSPRK) [4] for linear problems and the fourth order SSPRK(5,4) for nonlinear problems. The major advantage of the seventh order HWENO scheme is its compactness in the reconstruction. Five points only are needed in the stencil for the seventh order HWENO scheme while seven points are needed for the seventh order classical WENO schemes. The main advantages of the new scheme are: it is more accurate, robust, high resolution and can be used for problems with non-convex fluxes.

The paper is organized as follow. In section 2 we describe the numerical scheme which used in this paper.In section3 we introduce our new seventh order HWENO reconstruction. In section 4 we review the derivation of the central-upwind flux [9,10]. The strong-stability-preserving Runge-Kutta methods of time discretization are briefly

reviewed in section 5. Eextension of the scheme for systems equations in two dimensions is described in section 6. Section 7 presents the results of number of numerical tests of our method

2. The numerical scheme

In this section we will describe the construction and implementation of the seventh order Hermite WENO scheme for hyperbolic conservation laws (1.1). Firstly, we consider the one dimensional scalar hyperbolic conservation laws in the form

$$u_t + [f(u)]_x = 0, \qquad u(x,0) = u_0(x), \qquad x \in (-\infty, \infty), t \in (0, \infty) \tag{2.1}$$

where u(x,t) is a conserved quantity and f (u) is the physical flux. Throughout this paper, we consider only uniform grids and use the following notations. Let $x_j = j\Delta x, x_{j\pm\frac{1}{2}} = x_j \pm \frac{1}{2}\Delta x, \quad t^n = n\Delta t, \quad u_j^n = u(x_j, t^n)$

and the cell $I_j = \left\lfloor x_{j-\frac{1}{2}}, x_{j+\frac{1}{2}} \right\rfloor$, where Δx and Δt are small spatial and time scales.

Let $v = u_x$ and $g(u,v) = f'(u)u_x = f'(u)v,$ then from (2.1) and its spatial derivative we have the following equations

$$\left.\begin{aligned} u_t + [f(u)]_x &= 0, \qquad u(x,0) = u_0(x) \\ v_t + [g(u,v)]_x &= 0, \quad v(x,0) = v_0(x) \end{aligned}\right\} \tag{2.2}$$

We define the cell averages of u and v as

$$\bar{u}_j(t) = \frac{1}{\Delta x}\int_{I_j} u(x,t)\,dx, \quad \bar{v}_j(t) = \frac{1}{\Delta x}\int_{I_j} v(x,t)\,dx$$

Integrating (2.2) with respect to x over the cell I_j produces the following system of ordinary differential equations (ODEs) for the variables $\bar{u}_j, \bar{v}_j$

$$\left.\begin{aligned} \frac{d}{dt}\bar{u}_j(t) &= -\frac{1}{\Delta x}\left\{F_{j+\frac{1}{2}} - F_{j-\frac{1}{2}}\right\} \\ \frac{d}{dt}\bar{v}_j(t) &= -\frac{1}{\Delta x}\left\{G_{j+\frac{1}{2}} - G_{j-\frac{1}{2}}\right\} \end{aligned}\right\} \tag{2.3}$$

where $F_{j+\frac{1}{2}}(G_{j+\frac{1}{2}})$ is the numerical flux F(G) at $x_{j+\frac{1}{2}}$ and time t.

Following the finite volume methodology for generating a numerical scheme, the fluxes for u and v are approximated according to

$$\left.\begin{aligned} F_{j+\frac{1}{2}} &\approx \hat{F}_{j+\frac{1}{2}} = \hat{F}_{j+\frac{1}{2}}(u^{-}_{j+\frac{1}{2}}, u^{+}_{j+\frac{1}{2}}) \\ G_{j+\frac{1}{2}} &\approx \hat{G}_{j+\frac{1}{2}} = \hat{G}_{j+\frac{1}{2}}(u^{-}_{j+\frac{1}{2}}, v^{-}_{j+\frac{1}{2}}, u^{+}_{j+\frac{1}{2}}, v^{+}_{j+\frac{1}{2}}) \end{aligned}\right\} \tag{2.4}$$

where $u^{\pm}_{j+\frac{1}{2}}(v^{\pm}_{j+\frac{1}{2}})$ are the numerical approximations to the functions u(v) at the left and right of the interface $x = x_{j+\frac{1}{2}}$.

The equation (2.3) is approximated by conservative schemes

$$\left.\begin{aligned} \frac{d}{dt}\bar{u}_j(t) &= -\frac{1}{\Delta x}\left\{\hat{F}_{j+\frac{1}{2}} - \hat{F}_{j-\frac{1}{2}}\right\} = L_j(u) \\ \frac{d}{dt}\bar{v}_j(t) &= -\frac{1}{\Delta x}\left\{\hat{G}_{j+\frac{1}{2}} - \hat{G}_{j-\frac{1}{2}}\right\} = M_j(u) \end{aligned}\right\} \tag{2.5}$$

The numerical fluxes $\hat{F}_{j+\frac{1}{2}}$ and $\hat{G}_{j+\frac{1}{2}}$ are required to be Lipschitz continuous functions of several neighbouring values u_j and v_j and also to be consistent with the physical fluxes f(u) and g(u,v).

The steps to follow in the implementation of the numerical scheme (2.5) can be described as follows:

1) the derivation of $u^{\pm}_{j+\frac{1}{2}}$ and $v^{\pm}_{j+\frac{1}{2}}$,

2) evaluating the numerical fluxes $F_{j+\frac{1}{2}}(G_{j+\frac{1}{2}})$ at the cell boundary $x_{j+\frac{1}{2}}$ as a monotone function of the left and right extrapolated values $u^{\pm}_{j+\frac{1}{2}}$ and $v^{\pm}_{j+\frac{1}{2}}$.

Here we use the central-upwind flux introduced in [9,10]. The flux is based on the use of more precise information about the local speeds of propagation. The main advantages of this flux are high resolution, due to smaller amount of dissipation, the simplicity and no Riemann solvers and characteristic decomposition involved. In section 4 we review the derivation of this flux.

3) the system of ODEs in time (2.5) can be solved by any stable ODE solver which retain the spatial accuracy of the semi-discrete scheme. Here we use the seventh order linear strong stability preserving Runge-Kutta (ℓsspRK) [4].

3. Reconstruction of $u^{\pm}_{j+\frac{1}{2}}(v^{\pm}_{j+\frac{1}{2}})$ by seventh order HWENO method

It is well known that the piecewise polynomial reconstruction is one of the building blocks of the numerical scheme (2.5). The reconstruction should be both high order accurate and essentially non-oscillatory. Here we describe the procedure of the seventh HWENO reconstruction for both $u^{\pm}_{j+\frac{1}{2}}$ and $v^{\pm}_{j+\frac{1}{2}}$.

3.1 Reconstruction of $u^{\pm}_{j+\frac{1}{2}}$ by seventh order HWENO method from cell average $\{\bar{u}_j, \bar{v}_j\}$

Here we reconstruct $u^{\pm}_{j+\frac{1}{2}}$ as follows:

Step 3.1.1 Hermite polynomials

Given the nodal values $\bar{u}_j$ and $\bar{v}_j$, we construct Hermite third degree polynomials $P_j^n(x), \quad j = 0,1,2,3$ over the stencils $S_0 = \{x_{j-2}, x_{j-1}, x_j\}$, $S_1 = \{x_{j-1}, x_j, x_{j+1}\}$, $S_2 = \{x_j, x_{j+1}, x_{j+2}\}$, $S_3 = \{x_{j-2}, x_{j-1}, x_j, x_{j+1}, x_{j+2}\}$ and a sixth degree polynomial Q(x) over the bigger stencil $\tau = S_0 \cup S_1 \cup S_2$. These polynomials should satisfy

$$\frac{1}{\Delta x}\int_{I_{j+i}} P_0(x)\,dx = u_{j+i}, \quad i = -2,-1,0, \qquad \frac{1}{\Delta x}\int_{I_{j-1}} P_0'(x)\,dx = v_{j-1}$$

$$\frac{1}{\Delta x}\int_{I_{j+i}} P_1(x)\,dx = u_{j+i}, \quad i = -1,0,1, \qquad \frac{1}{\Delta x}\int_{I_{j+1}} P_1'(x)\,dx = v_{j+1}$$

$$\frac{1}{\Delta x}\int_{I_{j+i}} P_2(x)\,dx = u_{j+i}, \quad i = 0,1,2, \qquad \frac{1}{\Delta x}\int_{I_{j+1}} P_2'(x)\,dx = v_{j+1}$$

$$\frac{1}{\Delta x}\int_{I_{j+i}} P_3(x)\,dx = u_{j+i}, \quad i = -2,-1,0,1,$$

$$\frac{1}{\Delta x}\int_{I_{j+i}} Q(x)\,dx = u_{j+i}, \quad i = -2,-1,0,1,2, \qquad \frac{1}{\Delta x}\int_{I_{j+i}} Q_2'(x)\,dx = v_{j+i}, \quad i = -1,1 \tag{3.1}$$

Since we only need the values of these polynomials at the cell boundary $x_{j+\frac{1}{2}}$ in terms of the cell averages, we derive the following expressions

$$\left.\begin{aligned}
P_0(x_{j+\frac{1}{2}}) &= \frac{1}{12}\left(-5u_{j-2}-14u_{j-1}+31u_j-18\Delta x\, v_{j-1}\right)\\
P_1(x_{j+\frac{1}{2}}) &= \frac{1}{24}\left(-u_{j-1}+8u_j+17u_{j+1}-6\Delta x\, v_{j+1}\right)\\
P_2(x_{j+\frac{1}{2}}) &= \frac{1}{12}\left(u_j+10u_{j+1}+u_{j+2}-6\Delta x\, v_{j+1}\right)\\
P_3(x_{j+\frac{1}{2}}) &= \frac{1}{12}\left(u_{j-2}-5u_{j-1}+13u_j+3u_{j+1}\right)\\
Q(x_{j+\frac{1}{2}}) &= \frac{1}{240}\left(-u_{j-2}-40u_{j-1}+134u_j+144u_{j+1}+3u_{j+2}-9\Delta x\, v_{j-1}-54\Delta x\, v_{j+1}\right)
\end{aligned}\right\} \quad (3.2)$$

Step 3.1.2 Linear weights

Now one can find the linear weights denoted by $\gamma_0,\gamma_1,\gamma_2,\gamma_3$, such that

$$Q(x_{j+1/2}) = \sum_{k=0}^{3}\gamma_k P_k(x_{j+1/2}),$$

with $\sum_{k=0}^{3}\gamma_k = 1$ for all the cell averages of u and v in the bigger stencil τ. This leads to

$$\gamma_0 = \frac{1}{20}, \gamma_1 = \frac{12}{20}, \gamma_2 = \frac{3}{20}, \gamma_3 = \frac{4}{20} \quad (3.3)$$

Step 3.1.3 Smoothness indicators

To measure the smoothness of the function $P_j(x)$ for the stencils S_j, we need to calculate the smoothness indicators β_j. The smaller the value of β_j, the smoother the function $P_j(x)$ in its target cell. Moreover, this is another key component introducing the smoothness indicators which change the linear weights obtained in step 3.1.2 to nonlinear weights, to ensure both accuracy in smooth cases and non-oscillatory performance when at least one of the small stencils contains a discontinuity of the function u(x). We take the same form of smoothness indicators as in [8]

$$\beta_j \equiv \sum_{k=0}^{3}\Delta x^{2k-1}\int_{x_{j-1/2}}^{x_{j+1/2}}\left(\frac{d^k}{dx^k}P_j(x)\right)^2 dx \quad (3.4)$$

The smoothness indicators are given by

$$\beta_0 = \frac{1}{64}(-3u_{j-2} - 16u_{j-1} + 19u_j - 9\Delta x\, v_{j-1})^2 + \frac{1}{3}(-u_{j-2} - u_{j-1} + 2u_j - 3\Delta x\, v_{j-1})^2 +$$
$$\frac{1}{320}(-u_{j-2} + u_j - 2\Delta x\, v_{j-1})(-39u_{j-2} - 160u_{j-1} + 1992u_j - 180\Delta x\, v_{j-1}),$$

$$\beta_1 = \frac{1}{256}(-3u_{j-1} - 20u_j + 23u_{j+1} - 10\Delta x\, v_{j+1})^2 + \frac{1}{12}(u_{j-1} - 2u_j + u_{j+1})^2 +$$
$$\frac{1}{1280}(-u_{j-1} + 4u_j - 3u_{j+1} + 2\Delta x\, v_{j+1})(-39u_{j-1} - 164u_j + 203u_{j+1} - 82\Delta x\, v_{j+1}),$$

$$\beta_2 = \frac{1}{64}(-19u_j + 16u_{j+1} + 3u_{j+2} - 6\Delta x\, v_{j+1})^2 + \frac{1}{3}(2u_j - u_{j+1} - u_{j+2} + 3\Delta x\, v_{j+1})^2 +$$
$$\frac{1}{320}(-u_j + u_{j+2} - 2\Delta x\, v_{j+1})(-104u_j + 80u_{j+1} + 24u_{j+2} - 48\Delta x\, v_{j+1}),$$

$$\beta_3 = \frac{1}{576}(5u_{j-2} - 27u_{j-1} + 15u_j + 7u_{j+1})^2 + \frac{1}{12}(u_{j-1} - 2u_j + u_{j+1})^2 +$$
$$\frac{1}{2880}(-u_{j-2} + 3u_{j-1} - 3u_j + u_{j+1})(41u_{j-2} - 243u_{j-1} + 123u_j + 79u_{j+1}), \qquad (3.5)$$

With the smoothness indicators $\{\beta_j\}_j$ in (3.5) and linear weights $\{\gamma_j\}_j$ in (3.3), we can now compute the nonlinear weights ω_j, j=0,1,2,3

$$\omega_j = \frac{\overline{\omega}_j}{\sum_{k=0}^{3}\overline{\omega}_k} \quad \text{where} \quad \overline{\omega}_k = \frac{\gamma_k}{(\varepsilon + \beta_k)^2}, \qquad k = 0,1,2,3 \qquad (3.6)$$

Here ε>0 is a small parameter used to avoid division by zero in the denominator. We use here $\varepsilon = 10^{-6}$ in all numerical examples. The final HWENO reconstruction is then given by

$$u^{-}_{j+1/2} = \sum_{k=0}^{3}\omega_k P_j(x). \qquad (3.7)$$

The reconstruction to $u^{+}_{j+1/2}$ is mirror symmetric with respect to x_j of the above procedure.

3.2 Reconstruction of the derivative values $v^{\pm}_{j+1/2}$

Here we use the same stencils in step 3.1.

Step 3.2.1 Hermite polynomials

We construct four fourth degree Hermite polynomials $P_j^n(x), \quad j=0,1,2,3$ on S_0, S_1, S_2 and S_3 respectively, and one seventh degree polynomial Q(x) on $\tau = S_0 \cup S_1 \cup S_2$, satisfying

$$\left.\begin{aligned}
&\frac{1}{\Delta x}\int_{I_{j+i}} P_0(x)\,dx = u_{j+i}, \quad i=-2,-1,0, && \frac{1}{\Delta x}\int_{I_{j+i}} P_0'(x)\,dx = v_{j+i}, \quad i=-1,0\\
&\frac{1}{\Delta x}\int_{I_{j+i}} P_1(x)\,dx = u_{j+i}, \quad i=-1,0,1, && \frac{1}{\Delta x}\int_{I_{j+i}} P_1'(x)\,dx = v_{j+i}, \quad i=-1,1\\
&\frac{1}{\Delta x}\int_{I_{j+i}} P_2(x)\,dx = u_{j+i}, \quad i=0,1,2, && \frac{1}{\Delta x}\int_{I_{j+i}} P_2'(x)\,dx = v_{j+i}, \quad i=0,1\\
&\frac{1}{\Delta x}\int_{I_{j+i}} P_3(x)\,dx = u_{j+i}, \quad i=-2,-1,0,1,2,\\
&\frac{1}{\Delta x}\int_{I_{j+i}} Q(x)\,dx = u_{j+i}, \quad i=-2,-1,0,1,2, && \frac{1}{\Delta x}\int_{I_{j+i}} Q_2'(x)\,dx = v_{j+i}, \quad i=-1,0,1
\end{aligned}\right\} \tag{3.8}$$

Since we only need the values of the derivatives of these polynomials at the cell boundary $x_{j+\frac{1}{2}}$ in terms of the cell averages, we derive the following expressions

$$\left.\begin{aligned}
P_0'(x_{j+\frac{1}{2}}) &= \frac{1}{4\Delta x}\left(-2u_{j-2}-7u_{j-1}+9u_j\right)+\frac{1}{4}\left(-8v_{j-1}+v_j\right)\\
P_1'(x_{j+\frac{1}{2}}) &= \frac{1}{8\Delta x}\left(3u_{j-1}-16u_j+13u_{j+1}\right)+\frac{1}{8}\left(v_{j-1}-3v_{j+1}\right)\\
P_2'(x_{j+\frac{1}{2}}) &= \frac{1}{4\Delta x}\left(-8u_j+8u_{j+1}\right)+\frac{1}{4}\left(17v_j-2v_{j+1}\right)\\
P_3'(x_{j+\frac{1}{2}}) &= \frac{1}{12\Delta x}\left(u_{j-1}-15u_j+15u_{j+1}-u_{j+2}\right)\\
Q'(x_{j+\frac{1}{2}}) &= \frac{1}{120\Delta x}\left(-4u_{j-2}+15u_{j-1}-188u_j+179u_{j+1}-2u_{j+2}\right)+\frac{1}{120}\left(-7v_{j-1}+70v_j-11v_{j-1}\right)
\end{aligned}\right\} \tag{3.9}$$

Step 3.2.2 Linear weights

As in step (3.1.2), we compute the linear weights $\gamma_0', \gamma_1', \gamma_2', \gamma_3'$, satisfying

$$Q'(x_{j+\frac{1}{2}}) = \sum_{k=0}^{3} \gamma_k' P_k'(x_{j+\frac{1}{2}}),$$

with $\sum_{k=0}^{3} \gamma_k = 1$ for all the cell averages of u and v in the bigger stencil τ . This leads to

$$\gamma_0' = \frac{1}{15}, \gamma_1 = \frac{9}{15}, \gamma_2 = \frac{2}{15}, \gamma_3 = \frac{3}{15} \tag{3.10}$$

Step 3.2.3 Smoothness indicators

We then compute the smoothness indicators $\beta_j, \quad j = 0,1,2,3$ as below

$$\beta_j \equiv \sum_{k=2}^{4} \Delta x^{2k-1} \int_{x_{j-1/2}}^{x_{j+1/2}} \left(\frac{d^k}{dx^k} P_j(x) \right)^2 dx \tag{3.11}$$

Since we reconstruct the first derivative rather than the solution itself, the summation begins from the second derivative to the fourth derivatives.

Therefore we get

$$\begin{aligned}
\beta_0 = {} & \frac{1}{625}(-9u_{j-2} - 9u_{j-1} + 18u_j - 30\Delta x\, v_{j-1} + 4\Delta x\, v_j)^2 + \frac{39}{196}(u_{j-2} + 8u_{j-1} - 9u_j + 8\Delta x\, v_{j-1} + 2\Delta x\, v_j)^2 + \\
& \frac{117}{500}(7u_{j-2} + 7u_j - 14u_j + 20\Delta x\, v_{j-1} + 2\Delta x v_j)^2 + \frac{1}{625}(7u_{j-2} + 7u_j - 14u_j + 20\Delta x\, v_{j-1} + 2\Delta x v_j) \\
& (66u_{j-2} + 66u_{j-1} - 132u_j + 18\Delta x\, v_{j-1} + 32\Delta x v_j),
\end{aligned}$$

$$\begin{aligned}
\beta_1 = {} & \frac{1}{4}(10u_{j-1} - 20u_j + 10u_{j+1} + 3\Delta x\, v_{j-1} - 3\Delta x\, v_{j+1})^2 + \frac{39}{16}(u_{j-1} - u_{j-1} + \Delta x\, v_{j-1} - \Delta x\, v_{j+1})^2 + \\
& \frac{585}{16}(-2u_{j-2} + 4u_j - 2u_j - \Delta x\, v_{j-1} + \Delta x v_{j+1})^2 + \frac{1}{8}(-2u_{j-2} + 4u_j - 2u_j - \Delta x\, v_{j-1} + \Delta x v_{j+1}) \\
& (-38u_{j-2} + 76u_{j-1} - 38u_j - 21\Delta x\, v_{j-1} + 21\Delta x v_{j+1}),
\end{aligned}$$

$$\begin{aligned}
\beta_2 = {} & \frac{1}{16}(-29u_j + 28u_{j+1} + u_{j+2} - 12\Delta x\, v_j - 18\Delta x\, v_{j+1})^2 + \frac{39}{4}(9u_j - 8u_{j+1} - u_{j+2} + 4\Delta x\, v_j + 6\Delta x\, v_{j+1})^2 + \\
& \frac{585}{16}(-5u_j + 4u_{j+1} + u_{j+2} - 2\Delta x\, v_j - 4\Delta x v_{j+1})^2 + \frac{1}{8}(-5u_j + 4u_{j+1} + u_{j+2} - 2\Delta x\, v_j - 4\Delta x v_{j+1}) \\
& (-149u_j + 124u_{j+1} + 25u_{j+2} - 66\Delta x\, v_j - 108\Delta x v_{j+1}),
\end{aligned}$$

$$\begin{aligned}
\beta_3 = {} & \frac{1}{64}(-u_{j-2} + 12u_{j-1} - 22u_j + 12u_{j+1} - u_{j+2})^2 + \frac{39}{144}(-u_{j-2} + 2u_{j-1} - 2u_{j+1} + u_{j+2})^2 + \\
& \frac{585}{576}(u_{j-2} - 4u_{j-1} + 6u_j - 4u_{j+1} + u_{j+2})^2 + \frac{1}{96}(u_{j-2} - 4u_{j-1} + 6u_j - 4u_{j+1} + u_{j+2}) \\
& (7u_{j-2} - 20u_{j-1} + 26u_j - 20u_{j+1} + 7u_{j+2}),
\end{aligned} \tag{3.12}$$

With the smoothness indicators $\{\beta_j\}_j$ in (3.12) and linear weights $\{\gamma_j\}_j$ in (3.10), we can now compute the nonlinear weights ω_j, j=0,1,2,3

$$\omega_j = \frac{\overline{\omega}_j}{\sum_{k=0}^{3} \overline{\omega}_k} \qquad \text{where} \quad \overline{\omega}_k = \frac{\gamma'_k}{(\varepsilon + \beta_k)^2}, \qquad k = 0,1,2,3 \tag{3.13}$$

The final HWENO reconstruction to $v^{-}_{j+1/2}$ is then given by

$$v^{-}_{j+1/2} = \sum_{k=0}^{3} \omega_k P'_j(x). \tag{3.14}$$

The reconstruction to $v^{+}_{j+1/2}$ is mirror symmetric with respect to x_j of the above procedure.

Remark : For systems cases as the Euler equations of gas dynamics, in order to avoid oscillations, both the reconstructions of $u^{\pm}_{j+1/2}$ and $v^{\pm}_{j+1/2}$ from u_j and v_j are performed in the local characteristic directions.

4. The central-upwind flux

In this section we summarize the derivation of the central-upwind flux presented in [9,10].

We consider the one dimensional system of hyperbolic conservation law

$$u_t + f(u)_x = 0, \quad u(x,0) = u_0(x), t \geq 0, \quad x \in \Omega \tag{4.1}$$

Here u(x,t) is the vector of unknown conservative variables and f(u) is the physical flux vector.

We first reconstruct a conservative non-oscillatory piecewise polynomial interpolation $P_j(x)$, $x \in I_j$ from u^n_j, for each cell I_j. The piecewise polynomial reconstructions are, in general, discontinuous at the cell interfaces, $x = x_{j+1/2}$ and therefore their evolution is locally described by the solutions of generalized Riemann Problems. The sizes of the corresponding Riemann fans are determined by the right and left sided local speeds of propagation, $\{a^{\pm}_{j+1/2}\}$, which can be estimated by

$$\begin{aligned} a^{+}_{j+1/2} &= \max\left\{\lambda_N\left(\frac{\partial f(u^{-}_{j+1/2})}{\partial u}\right), \lambda_N\left(\frac{\partial f(u^{+}_{j+1/2})}{\partial u}\right), 0\right\} \\ a^{-}_{j+1/2} &= \min\left\{\lambda_1\left(\frac{\partial f(u^{-}_{j+1/2})}{\partial u}\right), \lambda_1\left(\frac{\partial f(u^{+}_{j+1/2})}{\partial u}\right), 0\right\} \end{aligned} \tag{4.2}$$

with $\lambda_1 < \ldots < \lambda_N$ being the eigenvalues of the Jacobian $\frac{\partial f}{\partial u}$.

Here, $u^{+}_{j+½} = P_{j+1}(x_{j+½})$, and $u^{-}_{j+½} = P_j(x_{j+½})$ are the corresponding right and left values of the piecewise polynomial interpolant $\{ P_j(x) \}$ at the cell interface $x = x_{j+½}$.

In the non-convex case, the formula (4.2) is incorrect if the flux convexity changes near $u^{\pm}_{j+½}$, and one should use a more accurate estimate of $\{a^{\pm}_{j+½}\}$ there. In this case, the speeds in (4.2) can be evaluated exactly:

$$a^{+}_{j+½} = \max_{u\in\left[u^{min}_{j+\frac{1}{2}},u^{max}_{j+\frac{1}{2}}\right]}\{f'(u),0\}, \quad a^{-}_{j+½} = \min_{u\in\left[u^{min}_{j+\frac{1}{2}},u^{min}_{j+\frac{1}{2}}\right]}\{f'(u),0\} \tag{4.3}$$

where $u^{min}_{j+½} = \min\left\{u^{-}_{j+½}, u^{+}_{j+½}\right\}$, $u^{max}_{j+½} = \max\left\{u^{-}_{j+½}, u^{+}_{j+½}\right\}$. For more details see [10].

The semi-discrete central-upwind scheme presented in [10] can be written as

$$\frac{d}{dt}u_j(t) = -\frac{1}{\Delta x}\left\{F_{j+\frac{1}{2}} - F_{j-\frac{1}{2}}\right\} = L_j(u) \tag{4.4}$$

The numerical flux is given by

$$F_{j+\frac{1}{2}} = \frac{a^{+}_{j+\frac{1}{2}} f(u^{-}_{j+\frac{1}{2}}) - a^{-}_{j+\frac{1}{2}} f(u^{+}_{j+\frac{1}{2}})}{a^{+}_{j+\frac{1}{2}} - a^{-}_{j+\frac{1}{2}}} + \frac{a^{+}_{j+\frac{1}{2}} a^{-}_{j+\frac{1}{2}}}{a^{+}_{j+\frac{1}{2}} - a^{-}_{j+\frac{1}{2}}}\left[u^{+}_{j+\frac{1}{2}} - u^{-}_{j+\frac{1}{2}}\right] \tag{4.5}$$

Notice that the accuracy of this scheme is determined by the accuracy of the reconstruction and the ordinary differential equation solver.

5. Time Discretization

The semi-discrete (2.5) is a system of time dependent ODEs, which can be solved by any stable ODE solver which retain the spatial accuracy of the scheme. It is useful to apply time discretization of the same order as the space discretization.

In this paper, we use linear strong-stability-preserving Runge-Kutta algorithm (ℓSSPRK) which are SSP for linear problems [4]. Here we used ℓSSPRK (m,m-1) i.e., m-stage and (m-1)th order method, developed by Gottlieb [4], whose coefficients can be determined recursively, up to the desired order of accuracy.

These Runge-Kutta methods are used to solve a system of ODEs

$$\frac{du}{dt} = L(u), \tag{5.1}$$

where L (u) is an approximation to the derivative $(-f(u)_x)$ in the differential equation (2.1).

This ℓSSPRK (m,m-1) method is given by:

$$\begin{aligned} u^{(0)} &= u^n \\ u^{(i)} &= u^{(i-1)} + \frac{1}{2}\Delta t\, L(u^{(i-1)}), \quad i = 1,\ldots,m-1 \\ u^{n+1} = u^{(m)} &= \sum_{k=0}^{m-2} \alpha_{m,k} u^{(k)} + \alpha_{m,m-1}(u^{(m-1)} + \frac{1}{2}\Delta t\, L(u^{(m-1)}) \end{aligned} \tag{5.2}$$

For the seventh order (m=8) $\alpha_{m,k}$ are given by

$$\alpha_{8,0} = \frac{2}{15}, \alpha_{8,1} = \frac{2}{7}, \alpha_{8,2} = \frac{2}{9}, \alpha_{8,3} = \frac{4}{15}, \alpha_{8,4} = 0, \alpha_{8,5} = \frac{4}{45}, \alpha_{8,6} = 0, \alpha_{8,7} = \frac{1}{315}$$

For general nonlinear problems, the ℓSSPRK (m, m-1) methods are no longer $o(\Delta t)^{m-1}$.

For these nonlinear problems we replace the linear SSPRK schemes with the five stage, fourth order nonlinear version SSPRK(5,4) given in [4]:

$$\begin{aligned} u^{(1)} &= u^n + 0.39175222\,\Delta t\, L(u^n) \\ u^{(2)} &= 0.444370494\,u^n + 0.5556295\,u^{(1)} + 0.36841059\,\Delta t\, L(u^{(1)}) \\ u^{(3)} &= 0.62010185\,u^n + 0.379898\,u^{(2)} + 0.25189177\,\Delta t\, L(u^{(2)}) \\ u^{(4)} &= 0.17807995\,u^n + 0.82192004\,u^{(3)} + 0.5449747\,\Delta t\, L(u^{(3)}) \\ u^{n+1} &= 0.5172317\,u^{(2)} + 0.0960597\,u^{(3)} + 0.3867086\,u^{(4)} + 0.063692\,\Delta t\, L(u^{(3)}) + 0.22600748\,\Delta t\, L(u^{(4)}) \end{aligned} \tag{5.3}$$

The stability condition for the above schemes is

$$CFL \le 1$$

where $CFL = \max_j \left(S_j^n \frac{\Delta t}{\Delta x} \right)$ is the Courant number. Here S_j^n is the maximum propagation speed in I_j at time level n.

6. The sixth order HWENO scheme for two dimensional conservation laws

In this section we extend the HWENO method presented in this paper to solve nonlinear two dimensional hyperbolic conservation laws. Consider the two dimensional scalar conservation laws:

$$u_t + [f(u)]_x + [h(u)]_y = 0, \qquad u(x,y,t) = u_0(x,y) \tag{6.1}$$

Where u(x,y,t) is a conserved quantity, f(u(x,y,t)) and h(u(x,y,t)) describe its flux in x-direction and y-direction. Let $v = u_x$ and $w = u_y$, taking the derivative x and y of (6.1) separately, then we obtain the complete equations form that we need to solve as below

$$\left.\begin{aligned} &u_t + [f(u)]_x + [h(u)]_y = 0, \\ &v_t + [g(u,v)]_x + [r(u,v)]_y = 0, \\ &w_t + [q(u,w)]_x + [s(u,w)]_y = 0, \end{aligned}\right\} \tag{6.2}$$

Where $g(u,v) = f'(u)v,\ r(u,v) = h'(u)v,\ q(u,w) = f'(u)w,\ s(u,w) = h'(u)w.$

Here we take the uniform mesh with the cell sizes $\Delta x = x_{j+\frac{1}{2}} - x_{j-\frac{1}{2}}, \Delta y = y_{j+\frac{1}{2}} - y_{j-\frac{1}{2}}$. We denote the cells $I_{ij} = \left[x_{i-\frac{1}{2}}, x_{i+\frac{1}{2}}\right] \times \left[y_{j-\frac{1}{2}}, y_{j+\frac{1}{2}}\right]$.

Again the conservative scheme for equation (6.2) may be written as a semi-discretization form

$$\left.\begin{aligned} &\frac{d\bar{u}_{i,j}(t)}{dt} + \frac{1}{\Delta x}\left\{\hat{f}_{i+\frac{1}{2},j} - \hat{f}_{i-\frac{1}{2},j}\right\} + \frac{1}{\Delta y}\left\{\hat{h}_{i,j+\frac{1}{2}} - \hat{h}_{i,j-\frac{1}{2}}\right\} = 0 \\ &\frac{d\bar{v}_{i,j}(t)}{dt} + \frac{1}{\Delta x}\left\{\hat{g}_{i+\frac{1}{2},j} - \hat{g}_{i-\frac{1}{2},j}\right\} + \frac{1}{\Delta y}\left\{\hat{r}_{i,j+\frac{1}{2}} - \hat{r}_{i,j-\frac{1}{2}}\right\} = 0 \\ &\frac{d\bar{w}_{i,j}(t)}{dt} + \frac{1}{\Delta x}\left\{\hat{q}_{i+\frac{1}{2},j} - \hat{q}_{i-\frac{1}{2},j}\right\} + \frac{1}{\Delta y}\left\{\hat{s}_{i,j+\frac{1}{2}} - \hat{s}_{i,j-\frac{1}{2}}\right\} = 0 \end{aligned}\right\} \tag{6.3}$$

We can straightforward extend the one dimension procedure to the numerical fluxes $\hat{f}_{i\pm\frac{1}{2},j}, \hat{g}_{i\pm\frac{1}{2},j}, \hat{h}_{i,j\pm\frac{1}{2}}$, and $\hat{s}_{i,j\pm\frac{1}{2}}$ in a dimension by dimension fashion. But it is difficult to approximate the mixed derivative terms $\hat{q} = [f'(u)w]_x$ and $\hat{r} = [h'(u)v]_y$ with the same order of accuracy. The question now is how to reconstruct the numerical fluxes for the mixed derivatives terms in (6.3),i.e., $\hat{q}_{i+\frac{1}{2},j}$ as a function of

$(u^{\pm}_{i+\frac{1}{2},j}, w^{\pm}_{i+\frac{1}{2},j})$ according to equation (4.4). To keep the compactness of the scheme, we construct $w^{\pm}_{i+\frac{1}{2},j}$ for fixed $y = y_j$ by fifth order WENO reconstruction, this leads to the two dimensional scheme is sixth order accuracy.

Firstly, we choose three small stencils $S_0 = \{x_{j-2}, x_{j-1}, x_j\}$, $S_1 = \{x_{j-1}, x_j, x_{j+1}\}$, $S_2 = \{x_j, x_{j+1}, x_{j+2}\}$ and big stencil $\tau = S_0 \cup S_1 \cup S_2$ at $y = y_j$. We interpolate the quadratic polynomials $P_j^n(x)$, $j = 0,1,2$ and fourth degree polynomial Q(x) such that

$$\left.\begin{aligned}
&\frac{1}{\Delta x}\int_{I_{i+k}} P_0(x)\,dx = u_{i+k,j} \quad k = -2,-1,0,\\
&\frac{1}{\Delta x}\int_{I_{i+k}} P_1(x)\,dx = u_{i+k,j} \quad k = -1,0,1\\
&\frac{1}{\Delta x}\int_{I_{i+k}} P_2(x)\,dx = u_{i+k,j} \quad k = 0,1,2,\\
&\frac{1}{\Delta x}\int_{I_{i+k}} Q(x)\,dx = u_{i+k,j} \quad k = -2,-1,0,1,2
\end{aligned}\right\} \tag{6.4}$$

A simple algebra leads to these polynomials at the cell boundaries $x_{j+\frac{1}{2}}$;

$$\left.\begin{aligned}
P_0(x_{j+\frac{1}{2}}) &= \frac{1}{6}\left(2u_{j-2} - 7u_{j-1} + 11u_j\right)\\
P_1(x_{j+\frac{1}{2}}) &= \frac{1}{6}\left(-u_{j-1} + 5u_j + 2u_{j+1}\right)\\
P_2(x_{j+\frac{1}{2}}) &= \frac{1}{6}\left(2u_j + 5u_{j+1} - u_{j+2}\right)\\
Q(x_{j+\frac{1}{2}}) &= \frac{1}{60}\left(2u_{j-2} - 13u_{j-1} + 47u_j + 27u_{j+1} - 3u_{j+2}\right)
\end{aligned}\right\} \tag{6.4}$$

The polynomial $Q(x_{j+1/2})$ can be written as a linear combination of the polynomials $P_0(x_{j+1/2}), P_1(x_{j+1/2})$ and $P_2(x_{j+1/2}),$ as follows

$$Q(x_{j+1/2}) = \sum_{k=0}^{2} \gamma_k P_k(x_{j+1/2}),$$

Where $\gamma_0, \gamma_1, \gamma_2$, are constants satisfying $\sum_{k=0}^{3} \gamma_k = 1.$ Therefore we obtain

$$\gamma_0 = \frac{1}{10}, \gamma_1 = \frac{6}{10}, \gamma_2 = \frac{3}{10} \tag{6.5}$$

The WENO procedure is to change the linear weights to nonlinear weights. This achieved through a choice of the so called smoothness indicators β_j

$$\beta_j \equiv \sum_{k=0}^{2} \Delta x^{2k-1} \int_{x_{j-1/2}}^{x_{j+1/2}} \left(\frac{d^k}{dx^k} P_j(x) \right)^2 dx$$

The smoothness indicators are given by

$$\beta_0 = \frac{1}{4}(u_{j-2} - 4u_{j-1} + 3u_j)^2 + \frac{13}{12}(u_{j-2} - 2u_{j-1} + u_j)^2$$

$$\beta_1 = \frac{1}{4}(-u_{j-1} + u_{j+1})^2 + \frac{13}{12}(u_{j-1} - 2u_j + u_{j+1})^2$$

$$\beta_2 = \frac{1}{4}(3u_j - 4u_{j+1} + u_{j+2})^2 + \frac{13}{12}(u_j - 2u_{j+1} + u_{j+2})^2 \tag{6.6}$$

With the smoothness indicators $\{\beta_j\}_j$ in (6.6) and linear weights $\{\gamma_j\}_j$ in (6.5), we can now compute the nonlinear weights ω_j, j=0,1,2

$$\omega_j = \frac{\overline{\omega}_j}{\sum_{k=0}^{2} \overline{\omega}_k} \quad \text{where} \quad \overline{\omega}_k = \frac{\gamma_k}{(\varepsilon + \beta_k)^2}, \qquad k = 0,1,2 \tag{6.7}$$

Then the approximation of $w^-_{i+1/2,j}$ is achieved as

$$w^-_{i+1/2,j} = \sum_{k=0}^{2} \omega_k P_k(x). \tag{6.8}$$

The reconstruction to $w^+_{i+1/2,j}$ is mirror symmetric with respect to x_j of the above procedure. Again, for system cases, the reconstruction procedure of $w^{\pm}_{i+1/2,j}$ are performed in the local characteristic directions.

To compute the mixed derivative term $r^{\pm}_{i,j+1/2}$, we perform the same procedure in y-direction.

7. Numerical Results

We compare the following schemes:

1- WENOB7: it is the classical seventh order WENO scheme presented in [1].

2- HWENO5 : it is the fifth order HWENO scheme presented in [11].

3- HWENO7: it is the seventh order HWENO scheme presented here.

For all examples we take CFL=0.4. Also, linear problems we use ℓSSPRK (m, m-1) method for time integration and for the nonlinear problems we replace the linear SSPRK schemes with SSPRK(5,4) method.

7.1 Accuracy Tests

We study the performance of our scheme by applying it to the following problems:

Example 1

We solve the transport equation

$$u_t + u_x = 0, \qquad x \in [-1,1] \tag{7.1}$$

subjected to periodic initial data

$$u(x,0) = \sin(\pi x) \tag{7.2}$$

with periodic boundary conditions. The output times are t = 2 and very long time t =1000.

The results obtained at t = 2, are shown in table 1. We note that WENOB7and HWENO7 schemes are seventh order accurate. We can see that the errors by HWENO7 are smaller than those by the classical WENO schemes.

To show the efficiency of our scheme, we compute the results at very long time t = 1000 and compare the results with the original schemes. Table 2 shows the results. It can be seen that our scheme is better than the others, even after a long time in L^1 norms and the size of errors.

7.2 Tests with shocks

Example 2.

We now consider the equation (7.1) with the initial condition [18]

$$u(x,0) = \begin{cases} \frac{1}{6}[G(x,z-\delta) + G(x,z+\delta) + 4G(x,z)], & -0.8 \le x \le -0.6 \\ 1, & -0.4 \le x \le -0.2 \\ 1 - |10(x-0.1)| & 0 \le x \le 0.2 \\ \frac{1}{6}[F(x,a-\delta) + F(x,a+\delta) + 4F(x,a)], & 0.4 \le x \le 0.6 \\ 0, & \text{otherwise} \end{cases} \tag{7.3}$$

Where $G(x,z)=\exp(-\beta(x-z)^2), F(x,a)=\{\max(1-\alpha^2(x-a)^2,0\}^{1/2}$,with periodic boundary condition on [-1,1]. The constants are taken as $a=0.5, z=-0.7, \delta=0.005, \alpha=10$ and $\beta=(\log 2)/36\delta^2$.

This initial condition consists of several shapes which are difficult for numerical methods to resolve correctly. Some of these shapes are not smooth and the other is smooth but very sharp. We compute the solution at t = 8 and very long time t = 2000. For comparison, firstly, we compute the solution at t= 8 on the mesh of 200 cells. Figure 1shows the results at t=8 of HWENO7 scheme. The full line is the exact solution and the symbols are the numerical solution. Comparing the results in figure 1 and the results in [1,11], we notice that the accuracy of HWENO7 is overall higher than that of the other schemes. In particular, HWENO7 provides better resolution of the discontinuous square pulse. We also note that the resolution of the left peak in HWENO7 is sharper. We notice also that HWENO7 scheme is more efficient, since its CFL=0.4 while in [11] CFL=0.2.To illustrate a long time behaviour of the resulting scheme, figures 2-4 show the results using WENOB7, HWENO5 and HWENO7 schemes for output time t = 2000. We observe that the results produced by WENOB7 and HWENO5 schemes are not satisfactory while HWENO7 scheme produces more accurate results for all parts of the solution, including the square pulse. This means that the use of central-upwind flux improves the accuracy and convergence of the scheme.

7.2.1 Example with non-convex flux

In this section we show the performance of the new method when used to solve the problems with non-convex fluxes.

Example 3. Buckley–Leverett's problem

Here we apply our schemes developed in this paper to Buckley–Leverett's problem, whose flux is non-convex:

$$\frac{\partial u}{\partial t}+\frac{\partial f(u)}{\partial x}=0, \qquad -1\le x\le 1, \qquad f(u)=\frac{4u^2}{4u^2+(1-u)^2}, \tag{7.4a}$$

subject to the initial condition

$$u_0(x)=\begin{cases}1 & x\in[-0.5,0],\\ 0 & \text{otherwise}\end{cases}, \tag{7.4b}$$

We have computed the solution at t = 0.4. Figure 5 shows the results obtained by HWENO7 scheme with N = 80. Comparing with the results in [11,12,13], it is noticed that HWENO7 scheme produces the most accurate for all

parts of the solution than the other schemes. We notice also that HWENO7 scheme is more efficient, since its CFL=0.4 while in [11] CFL=0.2.

7.3. Systems of equations

We apply our new schemes to the system of Euler equations of gas dynamics

$$U_t + F(U)_x = 0, \tag{7.5}$$

where $U = (\rho, \rho u, E)^T$ and $F(U) = (\rho u, \rho u^2 + P, u(E+P))^T$

where ρ is the density, u is the velocity, P is the pressure, $E = \frac{1}{2}\rho u^2 + \frac{P}{(\gamma - 1)}$ is the total energy and γ is the ratio of specific heats, taken as 1.4 here.

Example 4. Lax problem

We solve the Lax problem for Euler equations (7.5) and initial data consists of two states, left (L) and right (R)

$$(\rho_L, u_L, E_L) = (0.445, 0.311, 8.928) \quad \text{and} \quad (\rho_R, u_R, E_R) = (0.5, 0.0, 1.4275) \tag{7.6}$$

Separated by a discontinuity at x = 0.5.The computational domain is taken as the unit interval [0, 1]. Again we take 100 grid points. Figure 6 shows the performance of HWENO7 scheme at t= 0.16. Comparing with the results obtained in [11-13] we note that the HWENO7 scheme is still more accurate and efficient than the others.

Example 5 Shock / turbulence interaction problem

To show the advantages of our method, we will solve a problem with a rich smooth structure and a shock wave. A typical example for this is the problem of shock interaction with entropy waves.

We solve the Euler equations (7.5) with a moving Mach = 3 shock interacting with sine waves in density; i.e., initially [18]

$$\begin{aligned} (\rho_L, u_L, P_L) &= (3.857143, 2.629369, 10.3333), && \text{for} \quad x < -4 \\ (\rho_R, u_R, P_R) &= (1 + 0.2\sin 5x, 0, 1), && \text{for} \quad x > -4 \end{aligned} \tag{7.7}$$

The flow contains physical oscillations which have to be resolved by the numerical method. We compute the solution at t = 1.8. Figure 7 shows the computed density by HWENO7 scheme against the reference solution, which is a converged solution computed by the fifth order finite difference WENO scheme [8] with 2000 grid points. Here we use 200 grid points. Comparing the results in the figure with the results obtained in [11,12]with

300 grids and in [13] with 400 cells, we observe that our scheme are more accurate than the other schemes and more efficient than all the schemes since here we use 200 cells only

Example 6: Interacting Blast wave problem

The blast problem introduced by Woodward and Colella [16] is severe test problem and therefore a good problem to test the robustness of numerical schemes. This problem has the initial condition consists of three states

$$U(x,0)=\begin{cases}(\rho_L,u_L,P_L)=(1,0,1000), & x<0.1\\ (\rho_M,u_M,P_M)=(1,0,0.01), & 0.1<x<0.9\\ (\rho_R,u_R,P_R)=(1,0,100), & x>0.9\end{cases} \tag{7.8}$$

Boundary conditions are reflective. The solution of this problem contains the propagation of strong shock waves into low pressure regions, the collision of strong shock waves and interaction of shock waves and rarefactions, and is thus a good test of the schemes.

We display the numerical results of the density and velocity of this complex problem in figures 8-9. The results are with 200 cells at time t=0.028 and t= 0.038 and we get the exact solution from WENO scheme on 4000 cells.

Figures 8-9 show the density and velocity obtained by HWENO7 scheme. It is noticed that the HWENO7 scheme is able to obtain such sharp resolution of the complex double blast problem, particularly, the density peaks have almost the correct value. Again, comparing the given results with the results obtained with the scheme [12,13] with 800 cells we notice that our scheme is more accurate and more economic (200 cells).

7.4 Two dimensional Euler equations

The Euler equations governing unsteady compressible inviscid flows can expressed in conservation form as

We consider the two dimensional, Euler equations

$$U_t+[F(U)]_x+[G(U)]_y=0 \tag{7.9}$$

where $U=(\rho,\rho u,\rho v,E)^T$, $F(U)=(\rho u,P+\rho u^2,\rho uv,u(P+E))^T$, $G(U)=(\rho v,\rho uv,P+\rho v^2,v(P+E))^T$,

$P=(\gamma-1)\left[e-0.5\rho(u^2+v^2)\right]$, $S=\dfrac{P}{\rho^\gamma}$

In which ρ,P,S,e denote the density, the pressure, the entropy and specific total energy of the fluid, respectively. u and v are the velocity component in the x and y directions. γ is the ratio of the specific heats, and γ =1.4.

7.4.1 Double Mach reflection problem

The governing equation for this problem is the two dimensional Euler equations (7.9). The computational domain is $[0,4]\times[0,1]$. The reflecting wall lies at the bottom of the computational domain starting from $x=\frac{1}{6}$. Initially a right moving Mach 10 shock is positioned at $(x,y)=(\frac{1}{6},0)$ and makes 60° angle with the x-axis. For the bottom boundary, the exact post-shock condition is imposed from $x=0$ to $x=\frac{1}{6}$ and a reflective boundary condition is used for the rest of the x-axis. At the top boundary of the computational domain, the data is set to describe the exact motion of the Mach 10 shock; consult [16] for a detailed discussion of this problem. The output time is t=0.2. Figures 10 and 11 show the computed density by HWENO7 scheme on the 960×240 and 1920×480 cells. Comparing our results with those in the existing literature [11-13,16] it is seen that our scheme produces the flow pattern generally accepted at present as corrected, on all meshes. All discontinuities are well resolved and correctly positioned.

7.4.2. Two dimensional Vortex evolution problem

Here we check the accuracy of the present method in the two dimensions We solve the two-dimensional Euler equations with the initial conditions, corresponding to a smooth vortex, moving at 45^o to the Cartesian mesh lines in the square domain $[-5,5]\times[-5,5]$, see [1]. We apply periodic boundary conditions. The temperature and entropy are defined as $T=\frac{P}{\rho}$ and $S=\frac{P}{\rho^\gamma}$ with $\gamma=1.4$. The vortex is defined as the following isentropic perturbation to the uniform flow of unit values of primitive variables $(\rho,P,u,v)=(1,1,1,1)$:

$$u=1-\frac{\epsilon}{2\pi}e^{\frac{1}{2}(1-r^2)}y,\qquad v=1+\frac{\epsilon}{2\pi}e^{\frac{1}{2}(1-r^2)}x,$$

and the temperature

$$T==1-\frac{(\gamma-1)\epsilon^2}{8\gamma\pi^2}e^{(1-r^2)},\quad \frac{p}{\rho^\gamma}=1$$

where $r^2=x^2+y^2$ and the vortex strength is $\epsilon=5$. We compute the numerical solution at the output time t = 10 which corresponds to one time period; at this time the vortex returns to the initial position. Table 3 shows the

convergence study for the seventh order HWENO7 scheme with SSPRK(5,4) scheme for temporal and the ninth order MPWENO presented in [1] with the third order accurate Runge-Kutta scheme for time integral [1], we denote it as MPWENO9. The errors of the solution in L^1 norms are presented. We observe that HWENO7 scheme converges with approximately 5.6 order of accuracy while MPWENO9 scheme converges to approximately 4.8 order of accuracy. We notice that HWENO7scheme yields better accuracy in L^1 norms than MPWENO9 scheme, though the magnitude of errors become nearly the same.

7.4.3. Forward facing step problem

This is another popular case for high resolution schemes which has been proposed in [1], also called the Mach 3 wind tunnel test. The wind tunnel is 1 length unit wide and 3 length units long. The step is 0.2 length units high and is located 0.6 length units from the left hand end of the tunnel. The initial conditions are $(\rho, u, v, P) = (1.4, 3, 0, 1)$ which stand to a Mach 3 uniform flow impacting the step at the initial time. Supersonic inflow and outflow boundary conditions were applied at the left and right boundaries, respectively, while reflective wall boundary conditions were imposed on the lower and upper boundaries, respectively. The corner of the step is a singular point and we treat it the same way as in [1], which is based on the assumption of a nearly steady flow in the region near the corner. We compute the solution up to t=4 using (480×160) mesh elements. In figure 12, we show 30 equally spaced density contours from 0.54 to 6.15 computed by HWENO7 scheme with SSPRK(5,4). The scheme shows a good resolution to approximate the solution. Also, the results obtained by HWENO7 scheme are comparable to the results in [1].

REFERENCES

[1] D.S. Balsara and C-W. Shu " Monotonicity preserving weighted essentially non-oscillatory schemes with increasingly high order of accuracy" J. Comput. Physics 160 (2000) 405- 452

[2] R. Borges, M. Carmona, B. Costa, W. Sun Don, "An improved weighted essentially non-oscillatory scheme for hyperbolic conservation laws", J. Comput.Phys. 227 (2008) 3191–3211

[3] G. Capdeville, "A Hermite upwind WENO scheme for solving hyperbolic conservation laws ". J. Comput. Phys. 227, (2008) 2430-2454

[4] S. Gottlieb, "On high order strong stability preserving Runge–Kutta and multistep time discretizations", J. Sci. Comput. 25 (1) (2005) 105–128.

[5]A. Harten, "High resolution schemes for hyperbolic conservation laws" J.Comput.Phys. 49(1983) pp. 357-393

[6] A. Harten, Enqueist,B., Osher, S., and Chakravarthy, S.R., "Uniformly high order accurate essentially non oscillatory schemes" J.Comput.Phys. 71 (1987)pp 231-303.

[7] K. Henrick, T.D. Aslam, J.M. Powers, "Mapped weighted essentially non-oscillatory schemes: achieving optimal order near critical points", J. Comput. Phys. 207 (2005) 542–567.

[8] G.S. Jiang, and Shu, C.-W. "Efficient implementation of weighted ENO schemes", J. Comp. Phys. 126 (1996), 202–228

[9] A. Kurganov, Noelle, S., and Petrova, G. "Semi-discrete central-upwind schemes for hyperbolic conservation laws and Hamilton-Jacobi equations", SIAM J. Sci. Comp. 23 (2001), pp.707–740.

[10] A. Kurganov, G. Petrova, B. Popov, "Adaptive Semi-Discrete Central-Upwind Schemes for Nonconvex Hyperbolic Conservation Laws", SIAM J. Sci. Comput., 29 (2007), pp. 2381-2401

[11] H. Liu, Qiu, J.: Finite difference Hermite WENO schemes for conservation laws. J. Sci. Comput. **63**, 548–572 (2015)

[12] H. Liu, J. Qiu "Finite Difference Hermite WENO Schemes for Conservation Laws, II: An Alternative Approach", J Sci Comput. DOI 10.1007/s10915-015-0041-4 (2015)

[13] Z. Taoa, F. Lib, J. Qiu, " High-order central Hermite WENO schemes on staggered meshes for hyperbolic conservation laws" J.Comput.Phys. 281 (2015) 148–176

[14] J. Qiu, Shu, C.-W.: "Hermite WENO schemes and their application as limiters for Runge–Kutta Galerkin method: one-dimension case". J. Comput. Phys. **193**, 115–135 (2003)

[15]. J. Qiu, J., Shu, C.-W.: "Hermite WENO schemes and their application as limiters for Runge–Kutta discontinuous Galerkin method II: two-dimensional case". Comput. Fluids **34**, 642–663 (2005)

[16] Woodward, P., and Colella, P.," The numerical solution of two dimensional fluid flow with strong waves" J.Comput.Phys. 54(1984) pp 115-173

[17] Yousef H.Zahran, Mohammed M. Babatin, "Improved ninth order WENO scheme for hyperbolic conservation laws", Appl. Math. Comp., 219 (2013) 8198-8212.

[18] Yousef H. Zahran, "RCM-TVD hybrid scheme for hyperbolic conservation laws", Int. J. Numer. Meth. Fluids, 57(2007) 745-760.

N	WENOB7	WENOB7	HWENO5	HWENO5	HWENO7	HWENO7
	L^1 error	L^1 order	L^1 error	L^1 order	L^1 error	L^1 order
20	5.12E-7		5.52E-5		1.59E-8	
40	4.25E-9	6.91	1.49E-6	5.21	1.19E-10	7.07
80	3.38E-11	6.98	4.52E-8	5.04	8.78E-13	7.09
160	2.68E-13	6.98	1.40E-9	5.02	6.53E-15	7.07
320	2.10E-15	6.99	4.33E-11	5.01	4.76E-17	7.11

Table 1: Convergence study for equation (7.1) with initial condition (7.2) at t= 2

N	WENOB7	WENOB7	HWENO5	HWENO5	HWENO7	HWENO7
	L^1 error	L^1 order	L^1 error	L^1 order	L^1 error	L^1 order
20	5.05E-1		6.52E-1		9.73E-3	
40	2.63E-1	0.94	5.13E-1	0.35	1.36E-3	2.83
80	6.10E-2	2.11	1.34E-1	1.94	1.40E-4	3.29
160	7.35E-3	3.05	1.82E-2	2.88	7.93E-6	4.14
320	8.46E-4	3.12	2.60E-3	2.81	4.83E-7	4.03

Table 2: Convergence study for equation (7.1) with initial condition (7.2) at t= 1000

Mesh	MPWEN09	MPWEN09	HWEN07	HWEN07
	L^1 error	L^1 order	L^1 error	L^1 order
25×25	1.352E-2		1.366E-2	
50×50	1.988E-4	6.09	2.905E-4	5.55
75×75	3.757E-5	4.11	2.831E-5	5.74
100×100	1.073E-5	4.36	5.856E-6	5.48

Table 3. Convergence study for two dimensional vortex evolution problem

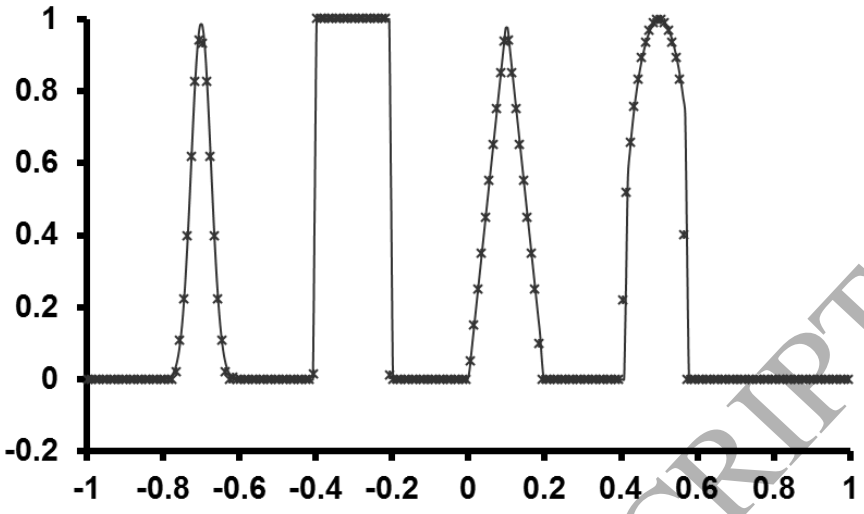

Figure 1. Solution of example 2 using HWENO7 scheme at t= 8

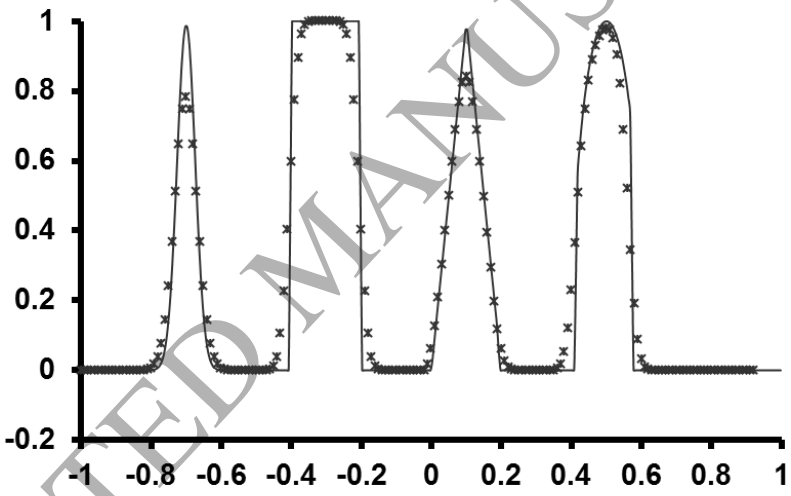

Figure 2. Solution of example 2 using WENOB7 scheme at t= 2000

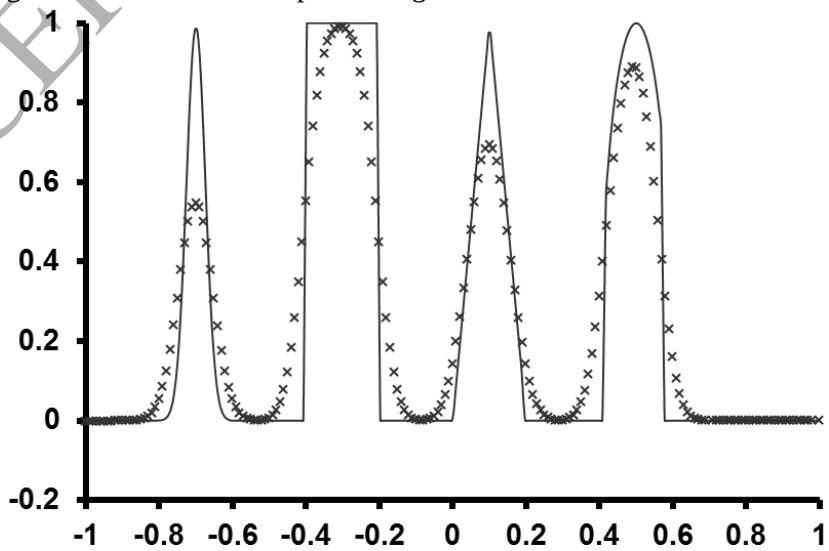

Figure 3. Solution of example 2 using HWENO5 scheme at t= 2000

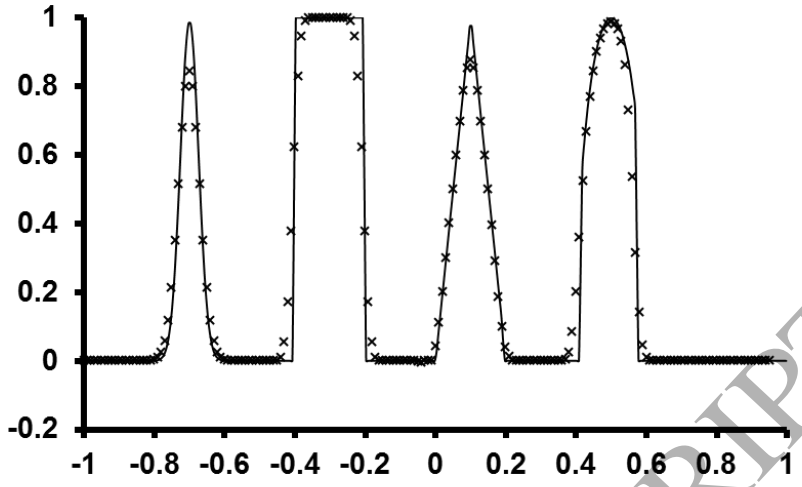

Figure 4. Solution of example 2 using HWENO7 scheme at t= 2000

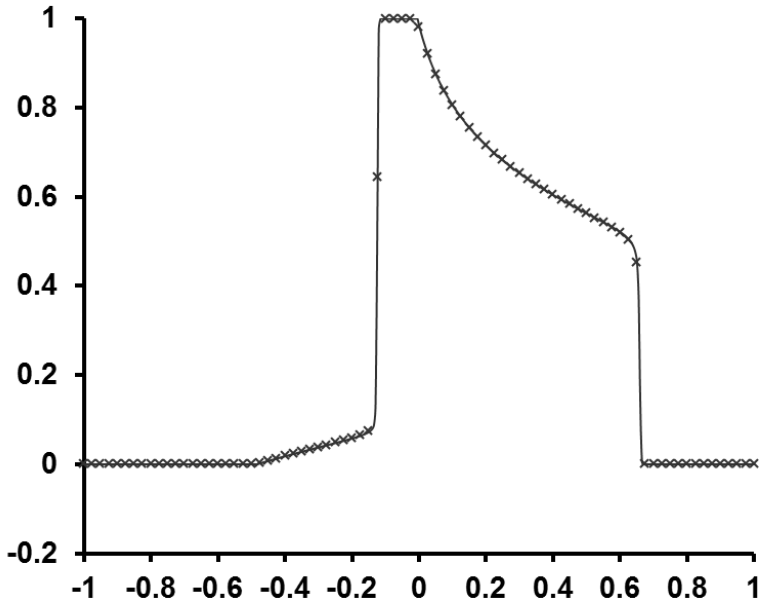

Figure 5. Solution of example 3 using HWENO7 scheme using SSPRK(5,4) time integration at t= 0.4

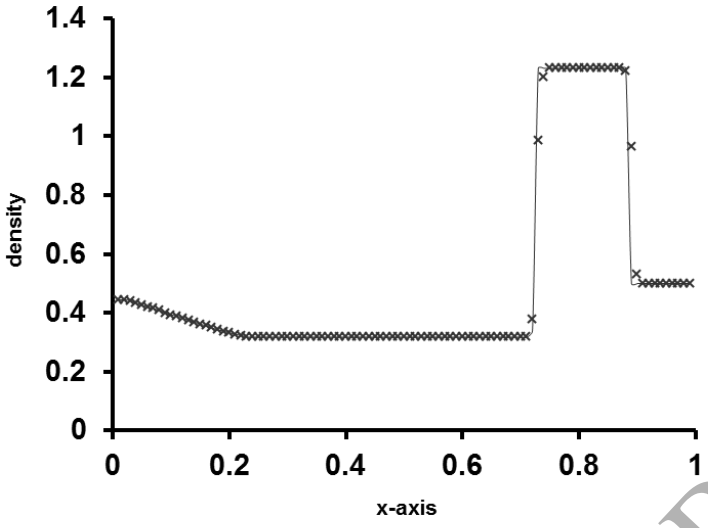

Figure 6. Solution of example 4 using HWENO7 scheme using SSPRK(5,4) time integration at t= 0.16

.

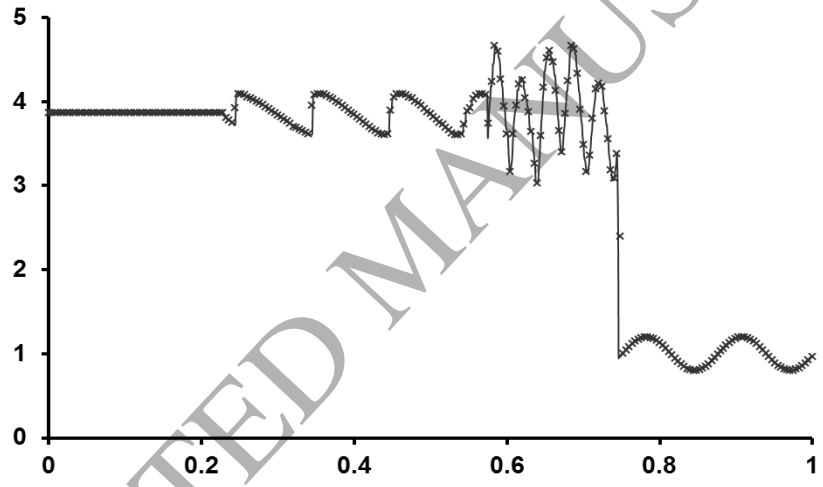

Figure 7. Solution of example 5 using HWENO7 scheme using SSPRK(5,4) time integration at t=1.8

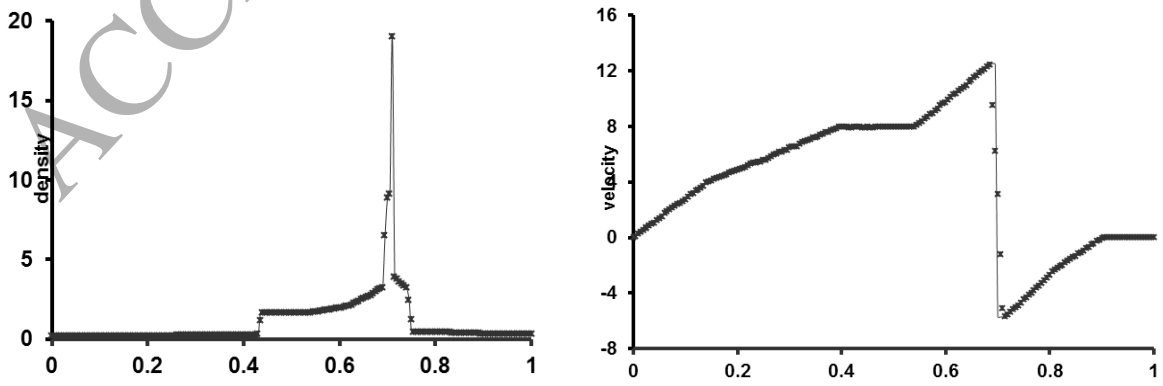

Figure 8. Solution of example 6 using HWENO7 scheme using SSPRK(5,4) time integration at t=0.028

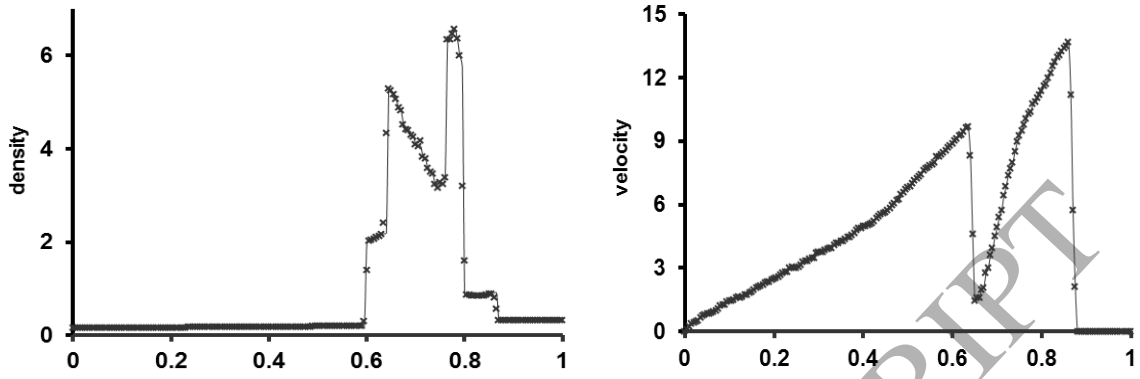

Figure 9. Solution of example 6 using HWENO7 using SSPRK(5,4) time integration scheme at t=0.038

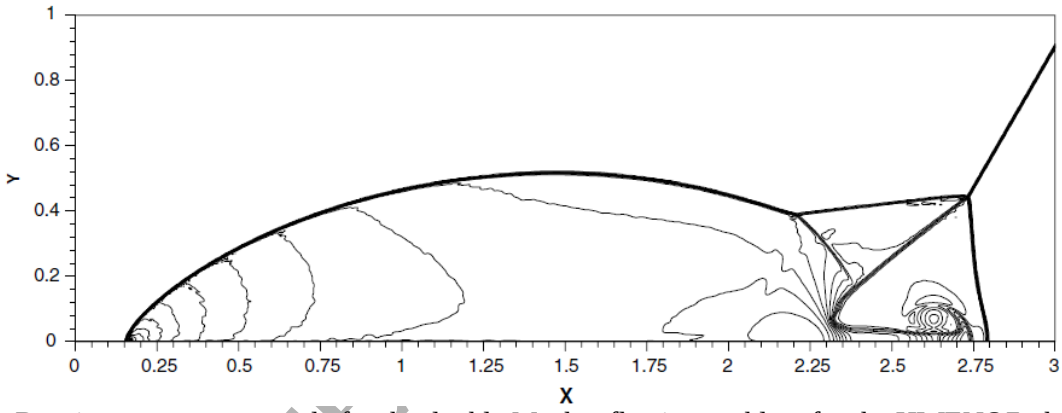

Figure 10. Density convergence study for the double Mach reflection problem for the HWENO7scheme, using SSPRK(5,4) time integration Meshes: 960×240 cells. 30 contour lines from 2 to 22.

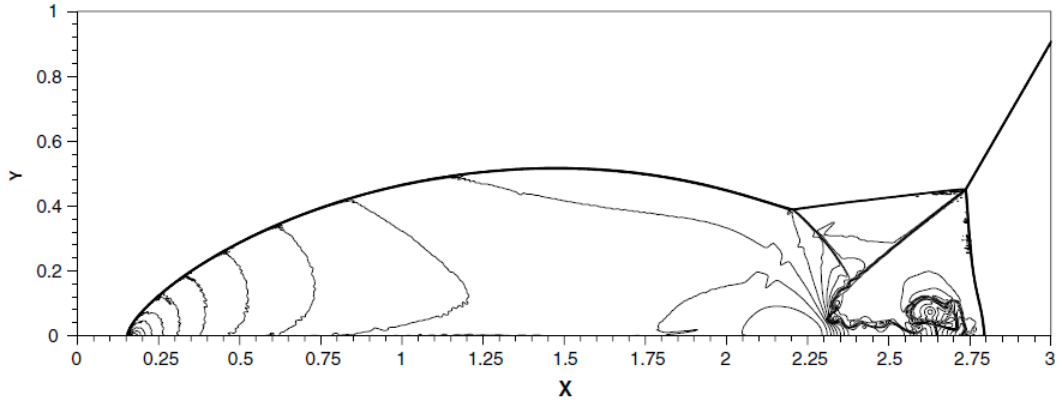

Figure 11. Density convergence study for the double Mach reflection problem for the HWENO7scheme, using SSPRK(5,4) time integration. Meshes: 1920×480 cells. 30 contour lines from 2 to 22.

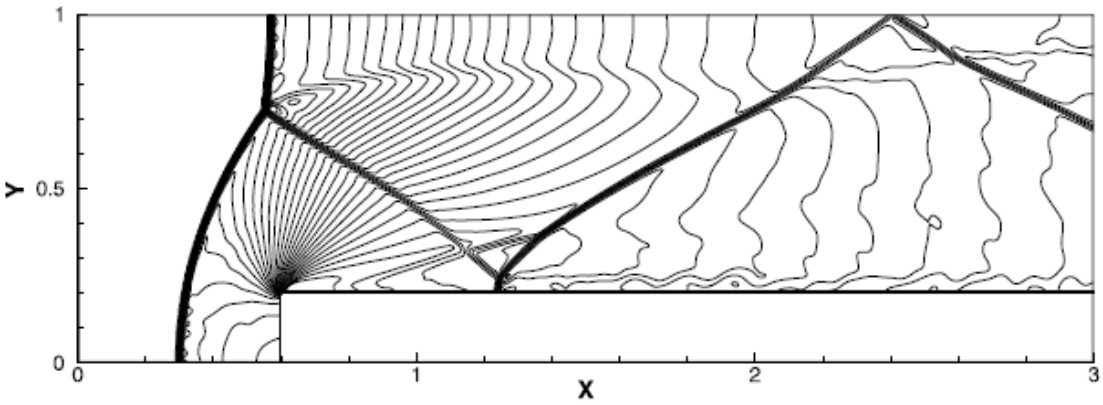

Figure 12. Forward facing step problem obtained by HWENO7 scheme using SSPRK(5,4) time integration with (480×160) cells , t=4. Thirty equally spaced density contours from 0.54 to 6.15.